

RESEARCH

Open Access



Predicting the compressive strength of ultra-high-performance concrete using a decision tree machine learning model enhanced by the integration of two optimization meta-heuristic algorithms

Runmiao Zhou¹, Yuzhe Tang², Hongmei Li^{3*} and Zhenni Liu¹

*Correspondence:
lihongmei@hatu.edu.cn

¹ Furong College, Hunan University of Arts and Science, Changde 415000, Hunan, China

² Hunan Technical College of Railway High-Speed, Hengyang 421200, Hunan, China
³ Information Engineering College, Hunan Applied Technology University, Changde 415000, Hunan, China

Abstract

The compressive strength (CS) of ultra-high-performance concrete (UHPC) hinges upon the distinct properties, quantities, and types of its constituent materials. To empirically decipher this intricate relationship, employing machine learning (ML) algorithms becomes indispensable. Among these, the decision tree (DT) stands out, adept at constructing a predictive model aligned with experimental datasets. Notably, these models demonstrate commendable accuracy, effectively paralleling experimental findings as a testament to DT's efficacy in UHPC prediction based on input parameters. To elevate predictive precision, this study integrates two meta-heuristic algorithms: the Sea-horse Optimizer (SHO) and the Crystal Structure Algorithm (CryStAl). This integration spawns three hybrid models: DTSH, DTCS, and DT. Particularly, the DTSH model shines with remarkable R^2 values, registering an impressive 0.997, coupled with an optimal RMSE of 1.746 during the training phase. This underlines the model's unmatched predictive and generalization capabilities, setting it apart from other models cultivated in this research. In essence, the fusion of empirical experimentation, advanced ML via DT, and the strategic infusion of SHO and CryStAl, culminates in the ascension of predictive prowess within the realm of UHPC compressive strength projection.

Keywords: Ultra-high-performance concrete, Compressive strength, Decision tree, Sea-horse Optimizer, Crystal Structure Algorithm

Introduction

Concrete is the foremost cement-based composite widely employed in construction projects [1]. However, the progressively intricate application contexts now demand heightened performance standards [2]. In response, ultra-high-performance concrete (UHPC), an innovative cement-based composite, has witnessed rapid advancement in recent years both in theoretical exploration and practical implementation [3]. UHPC demonstrates remarkable advantages in fulfilling the intricate requisites of modern construction,

encompassing lightweight structures, expansive spans, and national defence projects, owing to its exceptional mechanical attributes and enduring nature [4]. Diverging from conventional concrete types, UHPC's core objective to achieve outstanding performance revolves around cultivating a dense particle packing arrangement. Consequently, the incorporation of supplementary cementitious materials (SCMs) such as silica fume, fly ash, limestone powder, and metakaolin becomes necessary to fill voids among larger particles. This incorporation of SCMs, however, leads to a more intricate and variable UHPC mix, which in turn introduces instability in UHPC's performance, including mechanical characteristics, workability, and rheological properties. Thus, a fitting methodology for UHPC mix design becomes imperative [5–7].

However, traditional mix design approaches often rely on empirical knowledge and are sometimes offered without substantiation, lacking the guidance of particle packing theories. Currently, theoretical design approaches for UHPC predominantly stem from particle-dense packing models, categorizable into discrete and continuous models [8]. Discrete models assume a specific particle size set, whereas continuous models consider a continuous distribution of particle sizes seamlessly integrated into size distribution systems. In 2013, the American Society of Civil Engineers assigned a *D+* rating to the deteriorating US Infrastructure. Principal factors contributing to this decay are the corrosion of steel reinforcement and concrete degradation due to the infiltration of corrosive ions [9].

In comparison to standard concrete, *UHPC* stands out with substantial enhancements in mechanical and durability properties. *UHPC* holds the potential to address the prevailing state of dilapidated infrastructure effectively. A series of conferences held in Kassel, Germany [10–12]; Marseille, France [13]; and Des Moines, USA [14], have effectively showcased the material's performance and applicative prospects. Despite its impressive capabilities, the widespread adoption of UHPC faces obstacles arising from elevated material costs and sustainability concerns. The increased expenses stem from various factors intrinsic to UHPC, including the need for superior-quality materials, costly fibre reinforcements, and corresponding quality assurance [15]. Efforts have been undertaken to mitigate costs through the utilization of more affordable, locally available constituents.

Machine learning (ML) algorithms, like artificial neural networks (ANNs), have gained broad acceptance in various fields due to their ability to predict outcomes accurately, aligned with experimental results [16–18]. Nevertheless, experiments can involve intricate test matrices with many parameters, some of which contribute only minimally to the outcomes. In response, computer scientists have developed selection algorithms based on data-driven models [19–21]. These algorithms effectively identify the most relevant independent variables, swiftly reducing the dimensionality of the input matrix. The demand for soft computing tools in predictive modelling in engineering, covering components, systems, and materials, continues to rise steadily [22–24]. Among these tools, ANN has emerged as a leading soft computing approach, finding successful application across different engineering domains. ANN's usefulness extends to tasks such as prediction, approximation, character and pattern recognition, image processing, forecasting, classification, optimization, and control-related challenges. This versatility has motivated researchers to propose and utilize ANN models for a wide array of issues in

civil engineering. Notably, ANN behavioural modelling has been extensively employed to study concrete structural elements. Recent efforts have extended this research to employ various ANN models for predictive tasks related to building materials like steel, concrete, and composites [25]. Concrete, in particular, has garnered significant interest. ANN modelling, leveraging accumulated experimental data, has effectively addressed its fresh and hardened properties [26].

Additionally, predicting concrete's compressive strength has become a prolific area of investigation, where ANN models play a crucial role. The utilization of ANN for predicting the compressive strength of diverse concrete types, including normal weight, light-weight, and recycled, has intrigued researchers [27]. Simultaneously, exploring different ML techniques has enabled the comprehension of high-performance concrete's compressive strength. As the field has progressed, the introduction of UHPC has spurred further refinements in ANN modelling, broadening its application to predictive analyses of this cutting-edge material's behaviour [28].

The precision of UHPC prediction is being improved with the help of a novel ML technique introduced in this study. This primary focus is on obtaining extremely precise predictions of UHPC results, a crucial component in civil engineering. The study uses the decision tree (DT) model because collecting empirical data has inherent difficulties. However, careful parameter fine-tuning is essential to the DT model's success. The study uses a dual-algorithm approach that combines Sequential Halving Optimization (SHO) and Crystal Structure Analysis (CryStAl) to get the best performance possible from the DT model. This fusion turns out to be incredibly powerful, greatly improving the DT model's accuracy and efficiency. The practical benefits of this innovative strategy are especially notable in the infrastructure sector, where they simplify the design and construction of UHPC structures. With the aid of a sizable UHPC dataset, thorough comparative analyses are carried out to support the validity of this proposed framework. These results demonstrate a promising route for achieving precise UHPC forecasts in the context of civil engineering projects by incorporating the DT algorithm into this ML methodology.

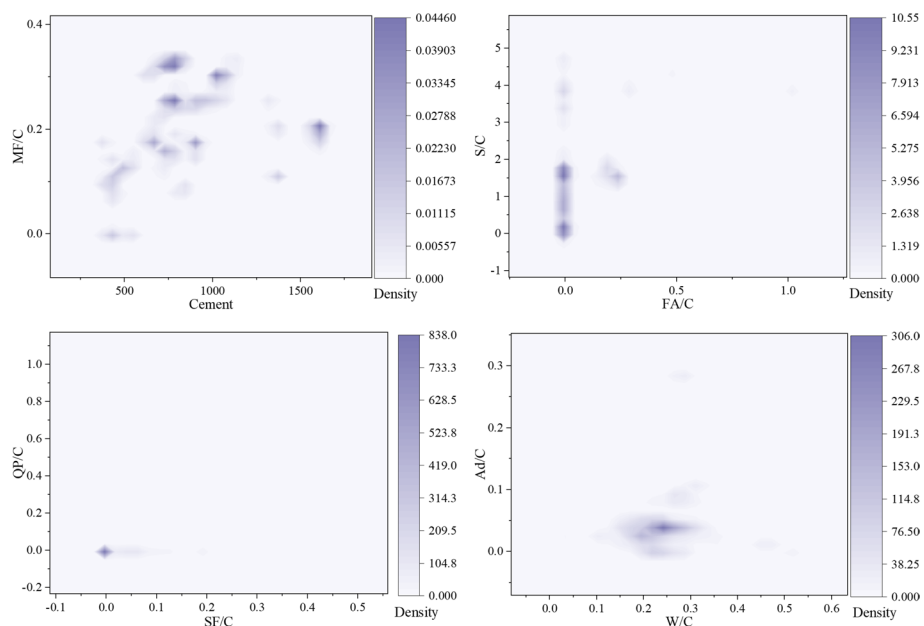
Methods

Data gathering

A meticulous approach assesses ultra-high-performance concrete (UHPC) within a soil context, considering numerous variables. The effort involves precise data management, dividing the dataset into training (70%), validation (15%), and testing (15%) subsets. The foundation is a dataset of 110 experimental samples from prior research, validating the empirical distribution method and fortifying predictive models. UHPC behaviour assessment and prediction utilize a decision tree (DT) model, leveraging inherent predictive capabilities within variables outlined in Table 1. The concrete mix design includes eight inputs: cement content (C), sand-cement ratio (S/C), silica fume-cement ratio (SF/C), fly ash-cement ratio (FA/C), steel fibre-cement ratio (STF/C), quartz powder-cement ratio (QP/C), water-cement ratio (W/C), and admixture-cement ratio (Ad/C). Except for cement (C), these inputs are as percentages relative to C . C is in (kg/m^3), while other inputs are percentages relative to C . The

Table 1 The properties of data set components engaged in the modelling process

Components	Units	Properties			
		Max	Min	Mean	St. dev
C	(kg/m ³)	1600	383	879.707	331.28
SF/C	(%)	0.332	0	0.214	0.0848
FA/C	(%)	1.011	0	0.053	0.1323
S/C	(%)	4.699	0	1.447	1.1751
STF/C	(%)	0.447	0	0.0395	0.076
QP/C	(%)	0.937	0	0.0469	0.157
W/C	(%)	0.514	0.0375	0.238	0.0636
Ad/C	(%)	0.281	0	0.0385	0.0399
CS	(MPa)	240	95	152.223	31.603

**Fig. 1** The 2D kernel plot between input and outputs

output, CS, quantified in megapascals (MPa), supports a robust comprehension of UHPC behaviour and predictive modelling insights. A 2D kernel plot, Fig. 1, visually illustrates input–output interplay. It represents associations between inputs and CS and depicts joint distribution or correlation. The plot shows pairs of data points, one axis showing input variables (e.g. cement content, S/C ratio) and the other CS values. Each point signifies an experimental sample with connected input and output. The plot aids in discerning trends, patterns, and interdependencies, identifying impactful input combinations on UHPC strengths. This representation helps researchers comprehend variable relationships and input–output impacts. Within the UHPC evaluation context, the 2D kernel plot enhances understanding of predictive model efficacy

by visually illustrating links between concrete mix design and compressive strength, enriching performance insight [29].

Decision tree (DT)

The (DT) is a widely used supervised learning technique for resolving classification and regression issues. When a specific categorical grouping or classification is absent, the regression analysis technique can still predict the likely outcome based on independent variables thanks to the hierarchy or divided structure of the tree [30, 31]. The model shown in Fig. 2 shows a straightforward decision tree with a single binary target variable, Y (with values of 0 or 1), two continuous variables, x_1 and x_2 , and all of their values fall between 0 and 1. Additionally, as shown in Fig. 3, the arrangement can be thought of as a segmented geographic area. The analytical framework that is frequently used includes dividing the sample space into distinct, well-defined, and comprehensive segments. Each of these segments directly relates to a particular leaf node, which denotes the result of a series of subsequent decision-making steps. Every record in a decision tree is given a single segment, called a leaf node, which serves as its home. Determining the most efficient model that can precisely segment all available data into distinct segments is the main goal of using decision trees for analysis [32].

Nodes and branches are the basic building blocks of a decision tree model, and splitting, stopping, and pruning procedures are important steps in its construction [33].

Nodes

Nodes fall into three distinct categories.

1. Primary nodes, called decision nodes, are the first category and denote a choice to partition or subset all data.

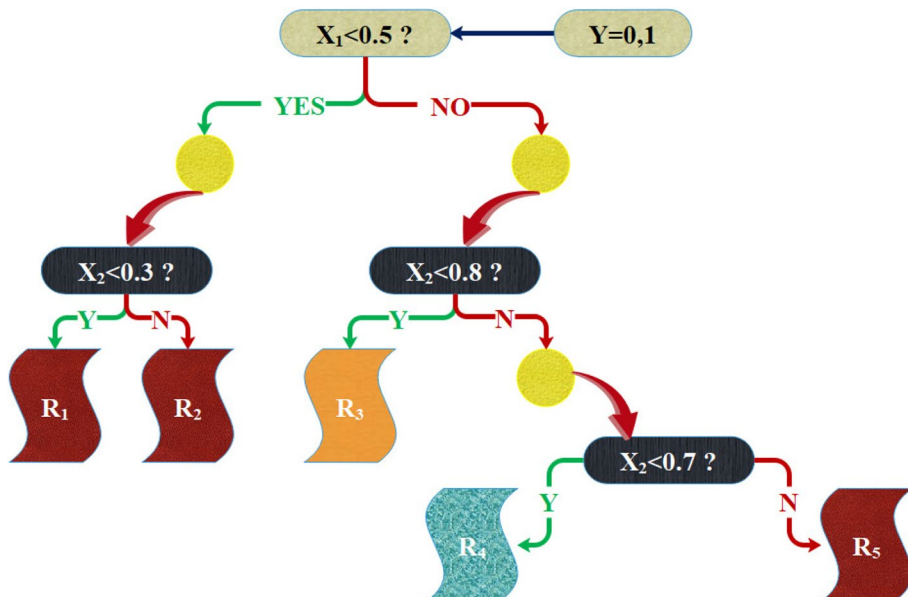


Fig. 2 Sample decision tree based on binary target variable Y

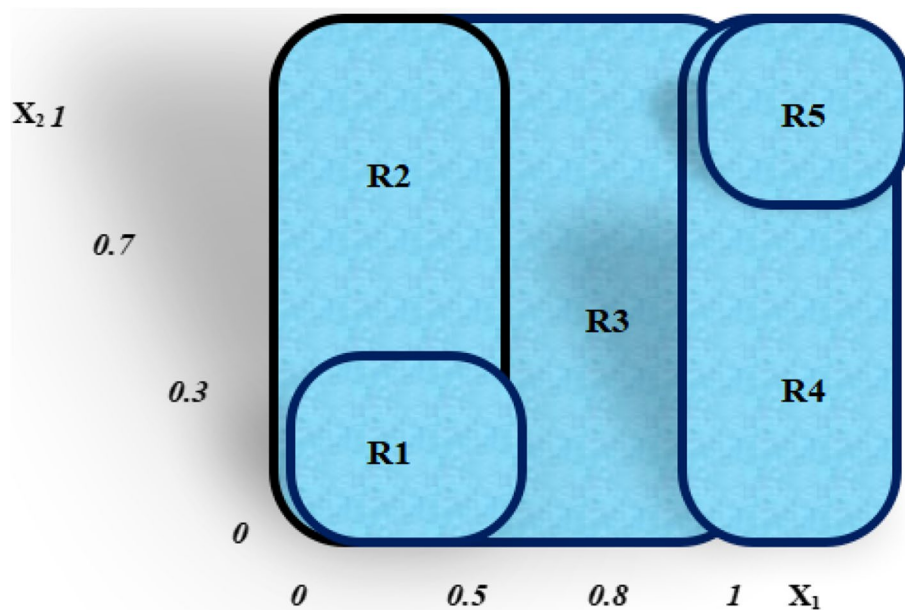


Fig. 3 DT using sample space view

2. An intermediary node, or chance node, is the second kind of node. It represents a constrained range of potential decisions that can be made at a specific location in the hierarchical structure.
3. Terminal nodes, also called end nodes, comprise the third category of nodes and represent the outcome of a string of assessments or events.

Branches

A hierarchical structure of branching elements represents chance events when building a decision tree model. A discrimination protocol can be expressed as rules using an if–then structure for each path from the root node through intermediary and terminal nodes. For instance, the realization of outcome j may depend on a series of conditions numbered from 1 to k , where the satisfaction of each condition causes outcome j to occur.

Splitting

It is necessary to identify key input variables and segment records based on them to build a model. The purity of the child nodes, determined by the percentage of the target condition, serves as a guide for choosing the input variables. The partitioning procedure is guided by metrics like entropy and the Gini index and continues until uniformity or stopping criteria are met. Most of the time, not all possible input variables are used, and a particular input parameter may be used more than once at different levels of the decision-making hierarchy.

Stopping

In statistical modelling, complexity and robustness must be balanced because they interact mutually antagonistically. The accuracy of future projections is inversely correlated with the model's complexity. Even though it is crucial to build a decision tree that matches current observations and has a small distribution of data points in each leaf, it is insufficient for forecasting future cases. Stopping rules must be incorporated during development to prevent excessive complexity. The number of observations needed in a leaf, the number of observations in a node before partitioning, and the depth measure are common parameters for stopping rules. Analytical goals and dataset characteristics must be thoroughly examined to choose the appropriate stopping parameters. Berry and Linoff recommend defining a specific percentage of records contained in a leaf node, ranging from 0.25 to 100%, regarding the entire training dataset to reduce overfitting and underfitting. A thorough approach is required to ensure the best accuracy and relevance in modelling.

Pruning

An alternative method for implementing stopping criteria in decision tree modelling entails growing a big tree and trimming it down to the perfect size by removing nodes that do not add much to the collection of new data. Utilizing the percentage of datasets linked to error prediction to choose the best subtree from a pool of candidates is a common technique. The ideal answer can be aided by validating the model on a different dataset. Pre-pruning and post-pruning are two acknowledged pruning techniques in machine learning. Pre-pruning involves using statistical tests such as chi-square [34] tests and multiple comparison adjustment techniques to limit the development of nonsignificant branches. Post-pruning, on the other hand, removes branches in an ideal way after building a thorough decision tree to increase classification accuracy when using the validation dataset. The specific context and features of the dataset will determine which pruning technique is used.

Sea-horse Optimizer (SHO)

In 2022, Zhao proposed a novel meta-heuristic approach called the SHO algorithm. The SHO algorithm is a population-based meta-heuristic technique that mimics the social behaviour of sea horses and consists of three primary components: movement, hunting, and reproduction. The algorithm incorporates both local and global search abilities to achieve a balance between exploration and exploitation capabilities. The movement behaviour is designed for local search, while the hunting behaviour is intended for global search, and the reproductive behaviour complements both [35]. The SHO algorithm commences by generating a population of potential solutions.

$$\text{SH} = \begin{bmatrix} x_1^1 \dots x_1^{\text{dim}} \\ \vdots \dots \vdots \\ x_{\text{pop}}^1 \dots x_{\text{pop}}^{\text{dim}} \end{bmatrix} \quad (1)$$

where dim represents the number of dimensions in the search space and pop indicates the population size used in the SHO algorithm, each member of the sea horse population represents a potential solution within the search space problem. In an optimization

problem that involves minimizing, the elite individual is determined as the one with the lowest fitness value and is denoted by X_{elite} . X_{elite} can be obtained using Eq. (2):

$$X_{elite} = argmin(f(X_i)) \quad (2)$$

The function $f(.)$ represents the cost function's value for a given problem, which assesses the fitness of potential solutions in the search space. The motion behaviour of sea horses involves two states: Brownian motion and Levy flight. Brownian motion facilitates enhanced exploration in the search space, while Levy flight simulates the step size of the movement of sea horses, allowing them to migrate and explore different locations to avoid excessive local exploitation. To determine the updated position of a sea horse in iteration t , we can express these two scenarios as follows:

$$X_{new}^2(t+1) = \begin{cases} X_i(t) + Levy(\lambda)((X_{elite}(t) - X_i(t)) \times x \times y \times z \times X_{elite}(t)r_1 > 0 \\ X_i(t) + rand * l * \beta_t * X_{elite}(t)r_1 < 0 \end{cases} \quad (3)$$

where $Levy$ is defined by the Lévy flight distribution function with a randomly generated parameter λ from the interval $[0, 2]$, the coordinates represent the spiral movement component of SHOtes x, y , and z . The constant coefficient l is used to control the step size of the Lévy flight; β_t is Brownian motion's random walk coefficient. The normal random number r_1 is used to introduce stochasticity in the Brownian motion component [36]. The hunting behaviour of sea horses can lead to either success or failure. Success is achieved when a sea horse captures its prey by moving faster, while failure results in further exploration of the search space. This hunting behaviour can be represented mathematically as:

$$X_{new}^2(t+1) = \begin{cases} b * (X_{elite} - rand * X_{new}^1(t)) + (1 - b) * X_{elite}(t)r_2 > 0.1 \\ (1 - b) * (X_{new}^1(t) - rand * X_{elite}) + b * X_{new}^1(t)r_2 < 0.1 \end{cases} \quad (4)$$

where the new location of the sea horse after hunting at iteration t is denoted as $X_{new}^1(t)$, r_2 is the randomly generated number within $[0, 1]$, and b is a directly decreasing parameter that adjusts seahorse-based step length during the hunting process. The reproductive behaviour of sea horses divides the population into male and female groups based on their fitness values, and male sea horses are responsible for reproduction.

$$mothers = X_{sort}^2(\frac{pop}{2} + 1 : pop) \quad (5)$$

where fathers and mothers refer to the male and female populations, respectively, while X_{sort}^2 denotes all X_{sort}^2 arranged in ascending order of their corresponding fitness values. The algorithm selects half of the best-fit individuals from the population to create a new generation of candidate solutions. The expression of the $i - th$ offspring is as follows:

$$X_i^{offspring} = r_3 X_i^{\text{father}} + (1 - r_3) X_i^{\text{mother}} \quad (6)$$

where r_3 is the random number between $[0, 1]$, X_i^{father} and X_i^{mother} individuals are chosen at random from the male and female populations. The SHO algorithm is specifically developed for solving optimization problems that entail continuous search spaces and

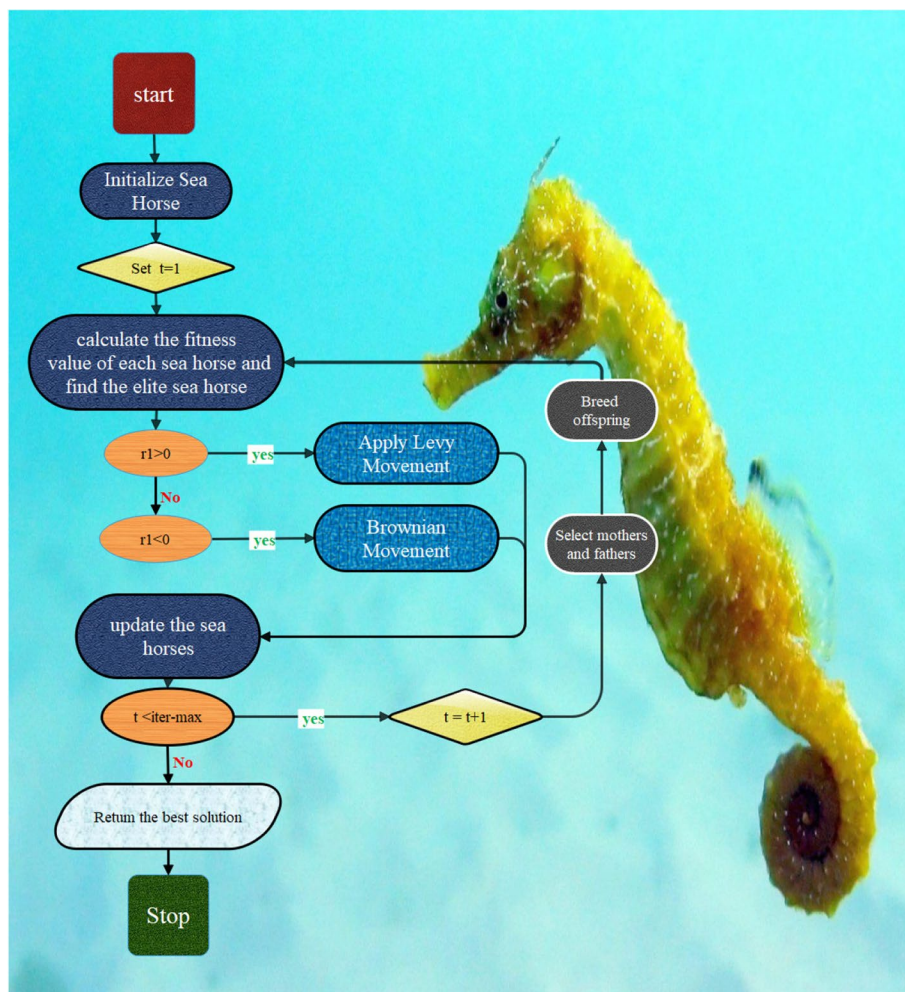


Fig. 4 The flowchart of the proposed SHO algorithm

has exhibited encouraging outcomes in several applications. The proposed SHO algorithm's flowchart is presented in Fig. 4.

The SHO algorithm offers a fresh perspective on resolving optimization problems, and its effectiveness and efficiency render it a promising technique for diverse applications.

Crystal Structure Algorithm (CryStAl)

Crystals are defined as minerals with a three-dimensional organized or regularly repeating crystalline structure. The sizes and forms of crystalline solids can vary, and they might have isotropic or anisotropic characteristics [37]. Crystals are made of tiny particles having a distinct form. Numerous chemical and physical compositions have been investigated and put forth via testing. Furthermore, human inventions like mechanics, buildings, and artwork have been impacted by the complex symmetries and qualities of crystals. The crystal structure is explained in this article using the Bravais model. This model takes the infinite lattice geometry into account, and it specifies the periodic structure that the lattice geometry describes together with the vector of the lattice locations in the following manner:

$$z = \sum s_i c_i \quad (7)$$

The lattice geometry and the vector of the lattice locations, where c_i is the minimum vector of the primary crystal directions and s_i is the angular number of the crystal, which explains the periodic structure in the Bravais model. This fundamental concept of crystals is described with suitable modifications for the mathematical modelling of *CryStAl*. In this paradigm, every possible optimization technique solution is thought of as a single crystal lattice. For the cycle's startup, any number of crystal lattices is chosen.

$$\begin{bmatrix} wz_1 \\ cwz_2 \\ \vdots \\ wz_i \\ \vdots \\ wz_s \end{bmatrix} = \begin{bmatrix} x_1^1 \dots x_1^j \dots x_1^q \\ x_2^1 \dots x_2^2 \dots x_2^q \\ \vdots \\ x_i^1 \dots x_i^2 \dots x_i^q \\ \vdots \\ x_s^1 \dots x_s^2 \dots x_s^q \end{bmatrix}, \begin{cases} i = 1, 2, 3, \dots, s \\ j = 1, 2, 3, \dots, q \end{cases} \quad (8)$$

where q is the problem's size, and s is the potential solution. The starting locations of these crystals in the search space are chosen at random by:

$$x_i^j(0) = x_{i,min}^j + \gamma (x_{i,max}^j - x_{i,min}^j), \begin{cases} i = 1, 2, 3, \dots, s \\ j = 1, 2, 3, \dots, q \end{cases} \quad (9)$$

The j th choice variable of the i -th candidate arrangement is within the indicated ρ , where $x_i^j(0)$ represents the beginning gem position and the least and maximum allowable values are characterized as $x_{i,max}^j$ and $x_{i,min}^j$ respectively. As to the crystallographic theory of the "base", all corner crystals make up the fundamental crystals. wz_{main} is randomly selected while taking into account the first crystal created. Furthermore, each tread has a random extraction technique defined, and the current value (z_l) is disregarded. wz_r indicates crystals having the ideal arrangement and D_v is the average of crystals that are chosen at random. Using basic network concepts, four kinds of update processes are created to track a candidate solution's location in the search space:

$$\text{Simplecubic } wz_{new} = wz_{main} + wz_{old} \quad (10)$$

$$\text{Bestcrystalcubicle } wz_{new} = z_1 wz_{zmain} + z_2 wz_r + wz_{old} \quad (11)$$

$$\text{Meancrystalcubicle } wz_{new} = z_1 wz_{zmain} + z_2 D_v + wz_{old} \quad (12)$$

$$\text{M&Bcrystalcubicle } wz_{new} = wz_{old} + z_1 wz_{zmain} + z_2 wz_r + z_3 D_v \quad (13)$$

In the above formula, the old position is given by wz_{old} , the new position is denoted by wz_{new} , and the random numbers are denoted by $z, z_1, z_2, \text{ and } z_3$. Metaheuristics consists of two main components: mining and exploration. It is noteworthy that Eqs. (10) to (13) have been tested to perform global and local searches simultaneously. To deal with variable solutions x_i^j that violate the variable limit requirements, a mathematical flag is created that requires adjustment of the variable limits, causing problems with x_i^j exceeding

the variable range. The termination criteria rely on a fixed number of iterations, after which the optimization process ends [38, 39].

Performance evaluation methods

In this study, various evaluation criteria for hybrid models are presented, emphasizing their correlation and error rates. The evaluation metrics discussed in this discussion include mean absolute error (MAE), coefficient of correlation (R^2), relative absolute error (RAE), root mean square error (RMSE), and Scatter Index (SI). The mathematical equations for each of these metrics are listed below. An algorithm with an R^2 value close to 1 performs exceptionally well in the training, validation, and testing phases. On the other hand, lower values of metrics like RMSE, RAE, and MAE are preferred because they signify a lower degree of model error.

$$R^2 = \left(\frac{\sum_{i=1}^N (h_i - \bar{h})(z_i - \bar{z})}{\sqrt{\left[\sum_{i=1}^N (h_i - \bar{h})^2 \right] \left[\sum_{i=1}^N (z_i - \bar{z})^2 \right]}} \right)^2 \quad (14)$$

$$RMSE = \sqrt{\frac{1}{N} \sum_{i=1}^N (z_i - h_i)^2} \quad (15)$$

$$MAE = \frac{1}{N} \sum_{i=1}^N |z_i - h_i| \quad (16)$$

$$SI = \frac{RMSE}{\text{mean}(z_i)} \quad (17)$$

$$RAE = \sum_{i=1}^N \frac{|z_i - h_i|}{|z_i - \bar{z}|} \quad (18)$$

The variables N , which stand for the number of samples, h_i , \bar{h} , and \bar{z} , which stand for the mean predicted and measured values, respectively, and z_i , which alternatively stands for the measured value, are used in Eqs. (14–18).

Results and discussion

This study's primary objective was to predict *UHPC* using three different models: DT, DTSH, and DTCS. During the training, validation, and testing phases, these models' performance was compared to actual measurements. Five statistical measures were used to ensure a thorough evaluation as indicated in Table 2: R^2 , RMSE, SI, RAE, and MAE. These metrics provided a solid basis for evaluating and contrasting the efficiency of the employed algorithms. The R^2 values, which measure how much of the variability in the dependent variable can be explained by the independent variable, received particular attention. A standout was the *DTSH* model, which achieved the highest R^2 values of 0.997 across all phases and displayed remarkable predictive accuracy. The DT model,

Table 2 Performance indices of proposed models

Models	DT			DTSH			DTCS			
	Section	Train	Validation	Test	Train	Validation	Test	Train	Validation	Test
RMSE		3.867	7.403	5.413	1.746	3.891	3.439	3.310	5.559	4.955
R^2		0.985	0.955	0.978	0.997	0.989	0.989	0.990	0.982	0.981
MAE		2.887	6.144	3.702	1.233	3.084	2.422	2.284	4.433	3.441
SI		0.025	0.051	0.035	0.011	0.027	0.022	0.022	0.038	0.032
RAE		26.357	27.025	26.64	12.824	66.650	16.50	23.669	69.721	21.44

on the other hand, produced slightly lower R^2 values, 0.985, during the corresponding phases. Beyond R^2 , the study also examined RMSE and other error indicators. The *DT* model showed more errors during the validation phase, with RMSE values ranging from 1.746 to 7.403, while the DTSH model showed the least errors during the training phase. The DTSH model obtained the lowest *SI* value of 0.011 during the training phase as part of the evaluation, indicating that it is the most suitable for modelling.

Similarly, the training phase of the *DT* model resulted in a *SI* value of 0.025. The DTSH model, which produced values of 1.233 and 12.824 for MAE and RAE during the training phase, emerged as the better choice compared to the *DT* model, which produced values of 2.887 and 26.357. Overall, the results convincingly demonstrate that the DTSH model is superior to the *DT* and *DTCS* models in all three stages. When selecting a model for real-world applications, it is crucial to consider additional aspects like model complexity, computational effectiveness, and ease of implementation. The study's findings essentially show that SHO optimization successfully enhances *DT*'s UHPC prediction capabilities. Therefore, using the DTSH model for actual UHPC prediction applications offers a useful and trustworthy option.

A scatter plot is used in Fig. 5 to compare a hybrid model's performance over the crucial training, validation, and testing phases. R^2 is used in the evaluation to determine how closely predicted and observed values are related, and RMSE is used to determine how much of a difference between the two there is. The DTSH model's central line and closely spaced data points show exceptional accuracy in all phases. Projected and actual value alignment reveals a remarkable agreement with few scattering traces. In contrast, despite having data points that are distributed more evenly around the central axis, the *DT* and *DTCS* models exhibit comparable performance levels. When compared to the DTSH model, this wider distribution suggests increased inaccuracy and relatively lower precision.

In Fig. 6, a comprehensive comparison is presented, demonstrating the correlation between predicted and measured *UHPC* through a bar chart plot. The evaluation of predictive precision is centred around how well the predicted and observed behaviours match. For the DTSH model, there is a subtle deviation across all three phases, with a notable concentration of predicted data points placed above their measured counterparts. Shifting to the *DT* and *DTCS* models, a slight difference becomes apparent between the projected and actual data points; however, their predictive accuracy falls slightly below the standard set by the DTSH model. On the contrary, the DTSH model's performance shows an even more modest alignment with the measured data

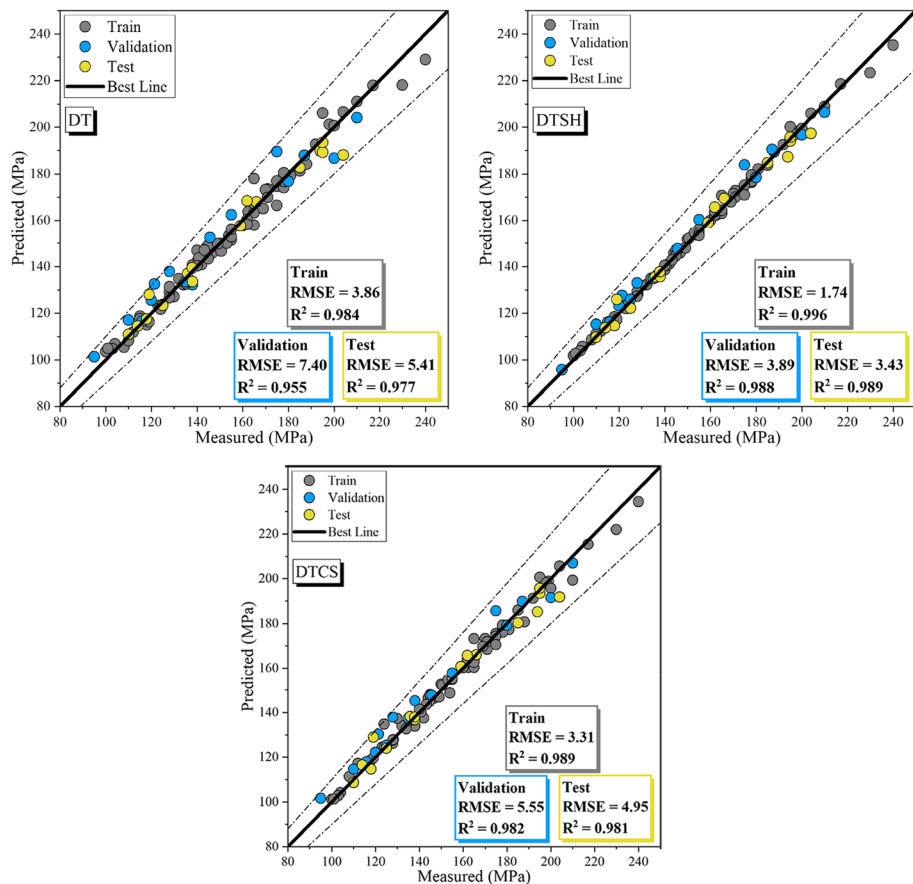


Fig. 5 The scatter plot for developed hybrid models

points than the other two models. This discrepancy is particularly evident, marked by a noticeable difference between the projected and observed values.

Figure 7 illustrates the error rate percentages of the hybrid frameworks using a normal distribution plot. These models underwent a comprehensive evaluation across three phases: training, validation, and testing, each with separate sample sets. The normal distribution plot vividly highlights notable differences in error distribution among the models. It is worth noting that the samples tend to cluster within a relatively narrow error range of -2 to 2% , showcasing the consistent and tightly grouped distribution exhibited by the DTSH model. The DTCS model displays an error rate of -3 to 3% , while the DT model shows a broader span of -5 to 5% , indicating its position as the model with the highest error rate. This observation emphasizes the consistent performance of the DTSH model across all evaluation phases. Among the trio of models, the DT model stood out due to its wider range of error percentages, indicating increased variability and reduced predictive precision compared to the other two models. Moving on, Fig. 8 presents a half-violin diagram depicting error percentages for the models in this study. During the training phase, DTSH exhibited an impressive mean error rate of 0% , characterized by a well-formed normal distribution with minimal dispersion. The error distribution consistently remained below the 6% threshold, indicating favourable results.

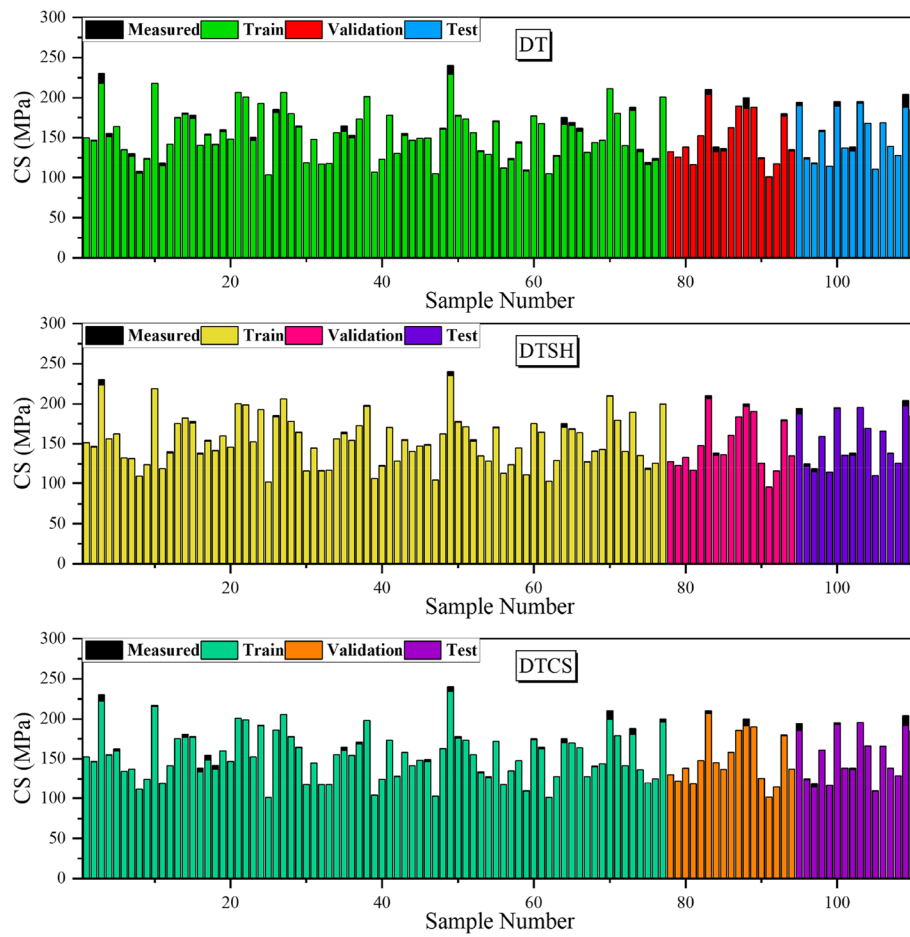


Fig. 6 The comparison of estimated and observed values

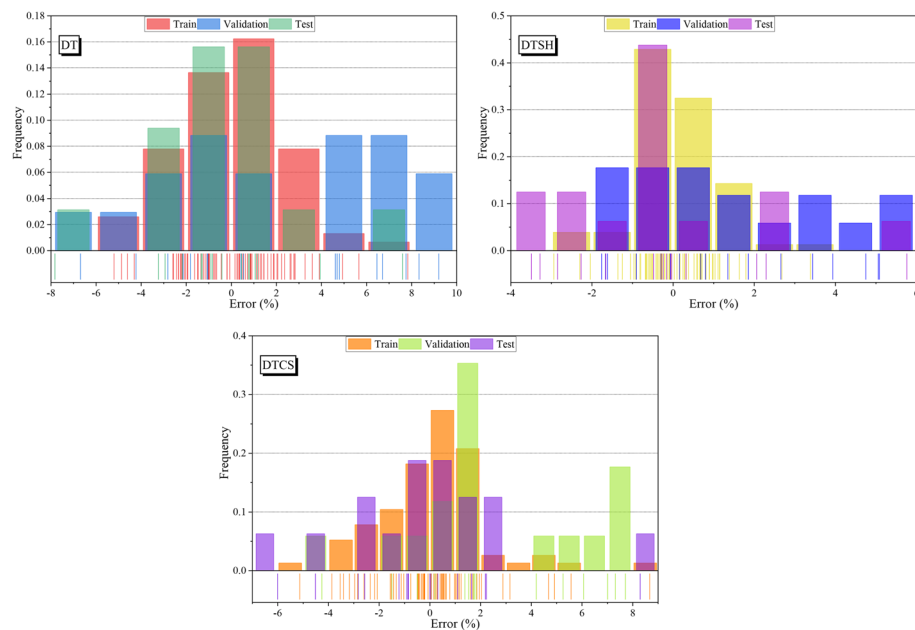


Fig. 7 The error rate percentage for the hybrid models is based on the normal distribution plot

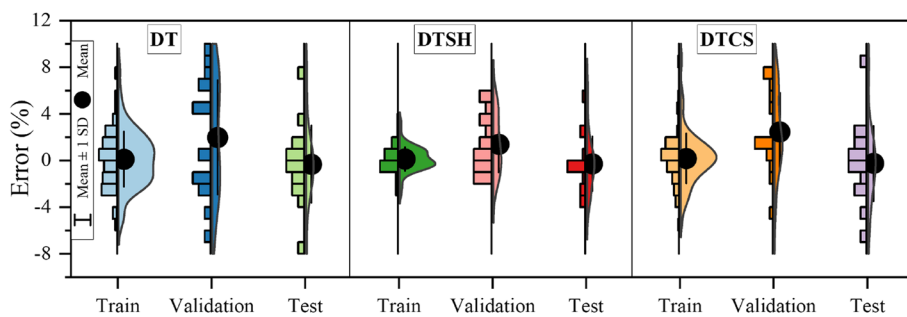


Fig. 8 The box of errors among the developed models

In contrast, the DT model displayed dispersion across both phases, featuring a symmetric and uniformly distributed normal curve. Despite this dispersion, the model managed to maintain its error percentage below 10%. DTCS showed the most pronounced and diverse discrepancies among the three models. Interestingly, a single outlier data point emerged during the assessment stage, comprising over 8% of the dataset, an unusual occurrence in statistical analysis. When considering dispersion, the DT model stood out, showing a greater spread than the other two models, with fewer instances of incidence near zero. Overall, all three models demonstrated satisfactory performance. However, DTSH showcased superior outcomes in terms of consistency and accuracy.

Conclusions

The number of experimental studies examining the characteristics of ultra-high-performance concrete (UHPC) has increased recently. However, using conventional statistical techniques to establish a precise relationship between the composition variables and the engineering features of UHPC has proven challenging and nonlinear. A robust and sophisticated approach is needed to make sense of the vast amount of experimental data available. This strategy ought to produce precise estimation methods and illuminate the complexities of nonlinear materials science. Enter ML, a potent technique that excels at spotting hidden patterns within complex datasets. In light of these considerations, the present study is dedicated to harnessing cutting-edge ML techniques, specifically DT, to predict the CS of UHPC. The foundation of this endeavour lies in a meticulously curated dataset consisting of 110 test experiments and 8 input parameters extracted from a comprehensive compilation of published literature. To elevate the predictive capabilities of the DT model, two meta-heuristic algorithms, SHO and CryStAl, have been seamlessly integrated. This amalgamation yields three distinct models: the original DT, an enhanced version DTSH empowered by SHO, and DTCS enriched by CryStAl. Evaluating these models is an exhaustive process, encompassing stages such as Training, Validation, and Testing. The dataset utilized for these evaluations comprises laboratory samples sourced from reputable published references. The efficacy and predictive prowess of the models in estimating UHPC compressive strength are quantified through an array of performance evaluation metrics, expounded upon in the dedicated section.

The culmination of these rigorous evaluations yields the following outcomes:

- a) According to the investigation, the DTSH variants of the models suggested in this study produced the most impressive results, showing the highest R^2 values. Even though the DT model had the lowest R^2 score, the difference was insignificant. The DTSH models outperformed the DT and DTCS models in terms of error rates, showing a notable 2% decrease in error rate in comparison to DTCS. The combined increased R^2 values and decreased error rates of the DTSH models highlighted their exceptional propensity for prediction.
- b) Notably, the DTSH model consistently displayed the lowest RMSE values across all phases, highlighting its remarkable dependability and accuracy in forecasting UHPC compressive strength. The RMSE of DTSH was noticeably 80% lower than that of the DT model, which is a resounding demonstration of the improved prediction accuracy of this method.

Acknowledgements

I would like to take this opportunity to acknowledge that there are no individuals or organizations that require acknowledgement for their contributions to this work.

Authors' contributions

All authors contributed to the study conception and design. Data collection, simulation and analysis were performed by RZ, YT, HL, and ZL. The first draft of the manuscript was written by HL, and all authors commented on previous versions of the manuscript. All authors read and approved the final manuscript.

Funding

This work was supported by the Key Project of Scientific Research Project of the Hunan Provincial Department of Education (22A0713).

Availability of data and materials

The authors do not have permissions to share data.

Declarations

Competing interests

The authors declare that they have no competing interests.

Received: 12 September 2023 Accepted: 20 December 2023

Published online: 14 February 2024

References

1. Nochaiya T, Wongkeo W, Chaipanich A (2010) Utilization of fly ash with silica fume and properties of Portland cement-fly ash-silica fume concrete. *Fuel* 89(3):768–774
2. Sun Y et al (2019) Understanding the porous aggregates carrier effect on reducing autogenous shrinkage of Ultra-High Performance Concrete (UHPC) based on response surface method. *Constr Build Mater* 222:130–141. <https://doi.org/10.1016/j.conbuildmat.2019.06.151>
3. Ragalwar K, Heard WF, Williams BA, Kumar D, Ranade R (2020) On enhancing the mechanical behavior of ultra-high performance concrete through multi-scale fiber reinforcement. *Cem Concr Compos* 105:103422. <https://doi.org/10.1016/j.cemconcomp.2019.103422>
4. Zhu Y, Zhang Y, Hussein HH, Chen G (2020) Flexural strengthening of reinforced concrete beams or slabs using ultra-high performance concrete (UHPC): a state of the art review. *Eng Struct* 205:110035
5. Yang R et al (2019) The physical and chemical impact of manufactured sand as a partial replacement material in Ultra-High Performance Concrete (UHPC). *Cem Concr Compos* 99:203–213. <https://doi.org/10.1016/j.cemconcomp.2019.03.020>
6. Yu R, Spiesz P, Brouwers HJH (2015) Development of an eco-friendly Ultra-High Performance Concrete (UHPC) with efficient cement and mineral admixtures uses. *Cem Concr Compos* 55:383–394. <https://doi.org/10.1016/j.cemconcomp.2014.09.024>
7. Ghafari E, Costa H, Júlio E (2015) Critical review on eco-efficient ultra high performance concrete enhanced with nano-materials. *Constr Build Mater* 101:201–208. <https://doi.org/10.1016/j.conbuildmat.2015.10.066>
8. Wang X et al (2019) Optimized design of ultra-high performance concrete (UHPC) with a high wet packing density. *Cem Concr Res* 126:105921. <https://doi.org/10.1016/j.cemconres.2019.105921>
9. Lehman M (2022) The american society of civil engineers' report card on america's infrastructure, in *Women in Infrastructure*. Midtown Manhattan, New York City: Springer, p 5–21.

10. Schmidt M, Fehling E, Geisenhanslüke C (2004) Ultra High Performance Concrete (UHPC): Proceedings of the international symposium on ultra high performance concrete. Kassel University Press, Kassel, Germany (September 13–15, 2004, no. 3)
11. Wille K, Naaman AE, Parra-Montesinos GJ (2011) Ultra-high performance concrete with compressive strength exceeding 150 MPa (22 ksi): a simpler way. *ACI Mater J* 108(1):46
12. Zhong R, Wille K, Viegas R (2018) Material efficiency in the design of UHPC paste from a life cycle point of view. *Constr Build Mater* 160:505–513
13. Toutlemonde F, Bernadi S, Brugeaud Y, Simon A (2018) Twenty years-long French experience in UHPFRC application and paths opened from the completion of the standards for UHPFRC, in The 2nd International Conference on UHPC Materials and Structures (UHPC2018-China) 24
14. Liu JP, Chen BC, Li C, Zhang MJ, Mou TM, Tabatabai H (2022) Recent application of and research on concrete arch bridges in China. *Struct Eng Int* 33:1–5
15. Wille K, Naaman AE, El-Tawil S, Parra-Montesinos GJ (2012) Ultra-high performance concrete and fiber reinforced concrete: achieving strength and ductility without heat curing. *Mater Struct* 45:309–324
16. Haykin S (2009) Neural networks and learning machines, 3/E. Chennai, India: Pearson Education India
17. Flood I (2001) Neural networks in civil engineering: a review. *Civ Struct Eng Comput* 2001:185–209
18. J. A. Abdalla, M. Attom, and R. Hawileh, Artificial neural network prediction of factor of safety of slope stability of soils, in Proceedings of the 14th International Conference on Computing in Civil and Building Engineering, 2012;27–29.
19. Abdalla JA, Attom MF, Hawileh R (2015) Prediction of minimum factor of safety against slope failure in clayey soils using artificial neural network. *Environ Earth Sci* 73:5463–5477
20. Das SK (2013) 10 - Artificial neural networks in geotechnical engineering: modeling and application issues, X.-S. Yang, A. H. Gandomi, S. Talatahari, and A. H. B. T.-M. in W. Alavi Geotechnical and Transport Engineering, Eds. Amsterdam, The Netherlands: Oxford: Elsevier, p 231–270. <https://doi.org/10.1016/B978-0-12-398296-4.00010-6>
21. Akbarzadeh MR, Ghafourian H, Anvari A, Pourhanasa R, Nehdi ML (2023) Estimating compressive strength of concrete using neural electromagnetic field optimization. *Materials (Basel)* 16(11):4200
22. Waszczyzyn Z, Ziemiański L (2001) Neural networks in mechanics of structures and materials—new results and prospects of applications. *Comput Struct* 79(22–25):2261–2276
23. Srisuksomwong P, Pekkoh J (2020) Artificial neural network model to prediction of eutrophication and microcystis aeruginosa bloom. *Emerg Sci J* 4(2):129–135
24. TavanaAmlashi A, MohammadiGolafshani E, Ebrahimi SA, Behnood A (2023) Estimation of the compressive strength of green concretes containing rice husk ash: a comparison of different machine learning approaches. *Eur J Environ Civ Eng* 27(2):961–983. <https://doi.org/10.1080/19648189.2022.2068657>
25. Hadi MNS (2003) Neural networks applications in concrete structures. *Comput Struct* 81(6):373–381
26. Khajeh A, Ebrahimi SA, MolaAbasi H, JamshidiChenari R, Payan M (2021) Effect of EPS beads in lightening a typical zeolite and cement-treated sand. *Bull Eng Geol Environ* 80(11):8615–8632. <https://doi.org/10.1007/s10064-021-02458-1>
27. Marani A, Nehdi ML (2020) Machine learning prediction of compressive strength for phase change materials integrated cementitious composites. *Constr Build Mater* 265:120286
28. Meenakshi M (2020) Machine learning algorithms and their real-life applications: a survey, in Proceedings of the International Conference on Innovative Computing & Communications (ICICC), Delhi, India
29. Abuodeh OR, Abdalla JA, Hawileh RA (2020) Assessment of compressive strength of ultra-high performance concrete using deep machine learning techniques. *Appl Soft Comput* 95:106552
30. Erdal HI (2013) Two-level and hybrid ensembles of decision trees for high performance concrete compressive strength prediction. *Eng Appl Artif Intell* 26(7):1689–1697
31. Ahmad A et al (2021) Prediction of compressive strength of fly ash based concrete using individual and ensemble algorithm. *Materials (Basel)* 14(4):794
32. Karbassi A, Mohebi B, Rezaee S, Lestuzzi P (2014) Damage prediction for regular reinforced concrete buildings using the decision tree algorithm. *Comput Struct* 130:46–56
33. Kotsiantis SB (2013) Decision trees: a recent overview. *Artif Intell Rev* 39:261–283
34. Zibrani MF (2007) Chi-squared test of independence. *Dep Comput Sci Univ Calgary Alberta Can* 1(1):1–7
35. Aribowo W (2023) A novel improved sea-horse optimizer for tuning parameter power system stabilizer. *J Robot Control* 4(1):12–22
36. Zhao S, Zhang T, Ma S, Wang M (2023) Sea-horse optimizer: a novel nature-inspired meta-heuristic for global optimization problems. *Appl Intell* 53(10):11833–11860. <https://doi.org/10.1007/s10489-022-03994-3>
37. Talatahari S, Azizi M, Tolouei M, Talatahari B, Sareh P (2021) Crystal structure algorithm (CryStAl): a metaheuristic optimization method. *IEEE Access* 9:71244–71261
38. Farooqui SA et al (2021) Crystal structure algorithm (CryStAl) based selective harmonic elimination modulation in a cascaded H-bridge multilevel inverter. *Electronics* 10(24):3070
39. Thomas JC, Natarajan AR, Van der Ven A (2021) Comparing crystal structures with symmetry and geometry. *Npj Comput Mater* 7(1):164

Publisher's Note

Springer Nature remains neutral with regard to jurisdictional claims in published maps and institutional affiliations.